Optical Materials xxx (xxxx) xxx

Contents lists available at ScienceDirect

Optical Materials

journal homepage: http://www.elsevier.com/locate/optmat

Study of various material particles by third harmonic generation method based on laser pulse induced plasma

Sandeep Kumar Maurya [a], Mottamchetty Venkatesh [a], Rashid A. Ganeev [a,b], Chunlei Guo [a,c,*]

[a] The Guo China-US Photonics Laboratory, State Key Laboratory of Applied Optics, Changchun Institute of Optics, Fine Mechanics and Physics, Chinese Academy of Sciences, Changchun, 130033, China
[b] Faculty of Physics, Voronezh State University, University Square, Voronezh, 394018, Russia
[c] The Institute of Optics, University of Rochester, Rochester, NY, 14627, USA

ARTICLE INFO

Keywords:
Third harmonic generation
Plasma
Particle characterization
Laser ablation

ABSTRACT

Third harmonic generation (THG) from plasma can be used as probe radiation to characterize the plasma components. In this work, we present the study of the spatiotemporal profile of generated particles in various plasmas produced from bulk targets (C, Cr, In, Ni, Ag, CdS and ZnS) using pulsed laser ablation and THG using 800 nm, 40 fs probe pulses. The dependence of THG on the probe pulse intensity and the distance of the probe beam from the target position are analyzed. The influence of the ejected particle mass on THG with respect to the distance between the target and the probe pulses position was observed. The temporal evolution of THG depended on the delay between heating 6 ns pulses and driving 40 fs pulses. The variation of third harmonic intensity in the plasma components with atomic weight M on the delay (t_d) was consistent with the kinetic model described by relation $t_d \propto M^{0.5}$. THG from metal targets was mostly originated from the atomic and ionic components in plasma, whereas the clusters and heavier particles were responsible for this process in the case of ablated semiconductor materials.

1. Introduction

The formation of nanoparticles with different shapes and sizes has attracted significant interest due to their potential applications in the nanotechnologies like biomedical imaging, environmental applications, and photonics materials synthesis for energy-based research [1–3]. Several methods are mentioned in literature for the formation of the nanoparticles, where the complete control over size and shape were achieved depending on the material characteristics [4–6]. Of various approaches for the preparation of nanoparticles, the laser ablation (LA) technique has been frequently used [7,8] because of the formation of neutral atoms, ions, clusters, and nanoparticles of different sizes during LA. The LA technique, which can be applied in almost all materials, provides high purity of prepared nanoparticles over other available techniques.

The generation of ejected particles strongly depends on the conversion of electronic and vibration excitation upon the interaction of the material with the laser pulses into the kinetic energy of particles motions. The LA process can be divided into three different steps including (a) bond-breaking and plasma ignition (b) plasma expansion and cooling, and (c) particle ejection and condensation. Plasma ignition process largely depends on the width of heating pulses. For nanosecond (ns) pulses, the plasma ignition process involves thermal vaporization, whereas, for picosecond (ps) pulses, it consists of both thermal and non-thermal mechanisms [9,10]. However, the Coulomb's explosion is responsible for plasma ignition in the case of femtosecond (fs) pulses through a bond-breaking mechanism [11]. The concentration of smaller particles size in the plasma is determined to be larger compared to large-sized particles [12]. The components of plasma have been widely studied using various technique [13,14]. Those techniques have been extensively implemented for the determination of the size, the shape, and the composition of plasma.

The clusters and nanoparticles have been recognized as the media possessing large optical nonlinearities. It has been proven that these multi-particle structures can be efficiently used for the generation of lower- and higher-order harmonics of ultrashort laser pulses [15–24]. The harmonic generation (HG) can be implemented as a characterization tool for the analysis of the composition of laser-induced plasmas.

* Corresponding author. The Guo China-US Photonics Laboratory, State Key Laboratory of Applied Optics, Changchun Institute of Optics, Fine Mechanics and Physics, Chinese Academy of Sciences, Changchun, 130033, China.
E-mail addresses: guo@ciomp.ac.cn, guo@optics.rochester.edu (C. Guo).

https://doi.org/10.1016/j.optmat.2019.109423
Received 17 July 2019; Received in revised form 23 September 2019; Accepted 25 September 2019
0925-3467/Published by Elsevier B.V.

The spatiotemporal separation of emitted particles during the formation of plasma has made HG an effective technique to characterize them. There are few reports on the usage of THG as a characterization scheme [25–27] for the generated particles in the plasma. This has been achieved by varying the arrival time of the probe pulses with respect to the heating pulses. The time delay based measurement of third harmonic (TH) emission has shown the presence of the larger aggregates formed during LA, which have been analyzed during their deposition on the nearby substrates [28,29].

The purpose of the present research is to investigate the role of physical characteristics of the bulk target on THG in various plasmas by introducing the variable delay between the heating and the probe pulses. Apart from time delay-based measurements, an alternative approach of probing the ejected particle during plasma formation is the measurement of the TH yield through the variation of the distance between the surface of the target and the probe pulses. Probing such particles in plasma through the measurement of TH can confirm the relationship between the mass and the velocity of the ejected particle during plasma creation similar to the delay based measurements. We use THG as a probe to identify the components of plasma from various bulk targets like graphite (C), silver (Ag), nickel (Ni), chromium (Cr), and indium (In), cadmium sulfide (CdS) and zinc sulfide (ZnS). THG in various plasmas is compared with the mass of the studied materials under vacuum conditions and in the air.

2. Experimental

All the bulk targets for the creation of plasma were used as purchased. We chose C (99.9%), Ag (99.95%), Ni (99.95%), Cr (99.95%), and In (99.95%) as the ablation targets. THG from wide-bandgap semiconductor materials, like CdS (99.95%), and ZnS (99.95%), were also carried out to observe the influence of the ejected particle mass on TH intensity.

The experimental setup for THG study consisted of the regenerative amplifier (Spitfire ACE, Spectra-Physics) operated at 800 nm with the repetition rate of 1 kHz and 40 fs pulse width. This system was seeded by Ti: sapphire oscillator (800 nm, 43 MHz, 60 nm bandwidth; Mai Tai, Spectra-Physics). Two different heating schemes were employed to perform THG in various targets. The first scheme [Fig. 1(a)] consisted of 200 ps heating pulses from the amplifier as a heating pulses to create plasma plume from the target. The second scheme [Fig. 1(b)] consisted of 6 ns heating pulses at 1064 nm with a repetition rate of 10 Hz (Q-smart 850, Quantel). The pulse width and beam diameter of the probe pulses at the position of the focusing lens were fixed at 40 fs and 20 mm, respectively. The beam diameters of ns and ps heating pulses were 5 and 7 mm respectively. The arrival time of the fs probe pulse in the plasma area was fixed at 38 ns from the beginning of ablation by ps heating pulses. In the case of ns heating, the arrival time of fs probe pulses with respect to heating pulse was controlled using a delay generator (DG535, Stanford Research Instruments). The delay generator was operated at 1 kHz using a trigger pulse from the amplifier. The heating pulses were focused on the targets using a 300 mm focal length lens, whereas the probe pulses were focused using a 500 mm focal length lens. The probes pulses were propagating parallel to the surface of the target as shown in Fig. 1. In the case of ps heating scheme, the focus point of the fs probe beam was set to be 2 mm away from the focal point of the heating beam as shown in the inset of Fig. 1(a). In the case of ns heating pulses, the focal points of both heating and probe pulses were set to be at the same point [see inset in Fig. 1(b)]. The energy of the heating pulses was fixed at 0.56 mJ for ps pulses and 3 mJ for ns pulses. The energy of probe pulses was varied by using a pair of a polarizer, and a half-wave plate with a maximum employed energy of 0.5 mJ. The pressure in the vacuum chamber was maintained at 0.1 Pa throughout the experiments for all samples. The generated TH radiation from the excited plasma was separated from the co-propagating fundamental beam using a prism and then was registered by a fiber spectrometer (Ocean Optics, USB 4000+). The target sample was moved with constant speed to get the stable TH intensity. To establish the contribution of plasma species to the THG, the plasma spectra were collected using a 100 mm fused silica lens, which focused the plasma emission on the tip of the optical fiber interfaced to the spectrometer.

3. Results and discussion

A systematic study was performed for the measurement of TH intensity in various plasmas, where the dependence of the TH emission on the power of probe pulses, position of the target with respect to the probe pulses, and as a function of the arrival time of the probe pulses with respect to the heating pulses was carried out. Our study consisted of two parts. The measurement of TH intensity in the air was performed using the scheme shown in Fig. 1(a), whereas the schematic in Fig. 1(b) was used to study the time evolution of TH in various plasmas by varying the arrival time of probe pulses with respect to heating pulses in vacuum condition.

3.1. THG from the metal plasmas produced in air

THG in the plasmas created on C, Ag and Ni targets in the presence of air was carried out to compare the role of ejected particles based on their mass. Prior to the measurement of TH in respective plasmas, THG in the air was measured as a function of the probe pulse energy up to 0.5 mJ, which shows the cubic dependence of HG on the probe pulse energy. The

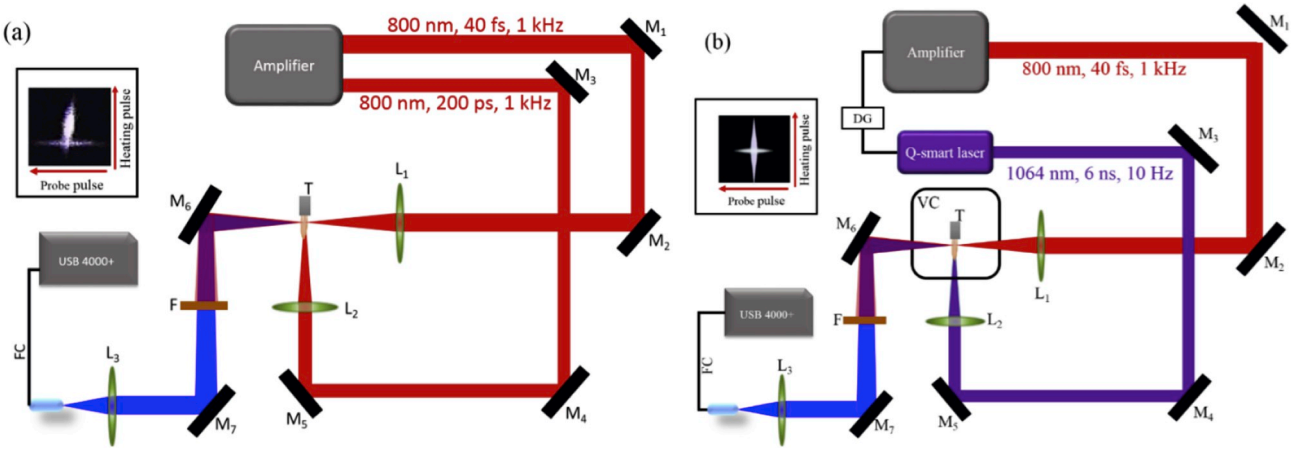

Fig. 1. Experimental setups for third-harmonic generation in (a) air and (b) vacuum conditions. M: mirrors, L: lenses, F: filter, T: target, VC: vacuum chamber, DG: delay generator. The insets show the spatial arrangements of the heating and probe laser pulses at the sample position in each schematic of the experimental setup.

intensity of TH from plasma was determined by subtracting the TH yield generated in the air from TH yield from plasma in the presence of air. As shown in Fig. 1(a), the wavelengths of the probe and heating pulses were kept at 800 nm with their respective pulse widths of 40 fs and 200 ps. The energy of the heating pulses was maintained at 0.56 μJ to create the plasmas. The arrival time of fs probe pulses was fixed at 38 ns after the beginning of plasma formation using ps heating pulses. The acquisition time for TH collection was kept at 10 s. The surface of the bulk target was placed ~2 mm away from the axis of propagation of the probe pulse. The spatial arrangement of the probe and the heating pulses at the target position is shown in the inset of Fig. 1(a), which can anticipate a significant difference in TH intensity with the variation of the distance between the probe pulses and the target. Fig. 2 shows the variation of TH intensity as a function of the distance between the axis of propagation of probe pulses and the surface of the target (C, Ag, Ni). TH intensity shows a similar profile as a function of the distance between the target position and the probe pulse with maxima at ~2 mm. The trend in the TH intensity variations with distance is related with the variation of heating laser fluence as the target moves away from the axis of probe pulse propagation due to the varying spot size of heating pulses on the target surface. The variation of spot size changes the fluence of heating pulses on the target surface during ablation therefore eventually producing the variable concentration of ejected particles as the target move towards the probe beam. The substantial difference was observed for the case of carbon plasma, which allowed observation of TH up to almost 4 mm away from the target position. This difference in TH yields from different plasmas is attributed to the difference in the masses of the ejected particles, assumed to be lighter for C compared to the heavier masses of the ejected particles from Ag and Ni targets. To support the effect of the mass of the ejected particle on TH intensity, the comparison of TH intensities in C plasma with respect to other heavier metal targets was analyzed under vacuum conditions, which is discussed later.

Fig. 3 shows the variation of TH intensity as a function of probe pulse energy at constant heating pulses energy of 0.56 mJ. The energy of probe pulses was varied between ~5 μJ and ~70 μJ. The surfaces of the bulk targets were placed 2 mm away from the probe pulses propagation to measure the influence of the pulse energy on TH yield. As shown in Fig. 3, the observed TH yield from C plasma is highest in comparison to Ag and Ni plasma at the constant probe pulse energy. The TH efficiency from plasma depends on the mass of the ejected particle during LA process in addition to the generated particle size distribution in plasma. It was demonstrated that the created plasma consists of a typical primary particle having a smaller diameter for C [30] and Ag [31,32] in addition to the atomization of the surface of the target. These particles contribute to the THG during ablation. The approximately cubic dependence of the yield of TH up to the probe pulse energy of 50 μJ was observed. As we further increased the energy of the probe pulses, the decrease of TH yield was observed in the case of Ag and Ni targets. This notable deviation from the cubic dependence can be attributed to the appearance of a large

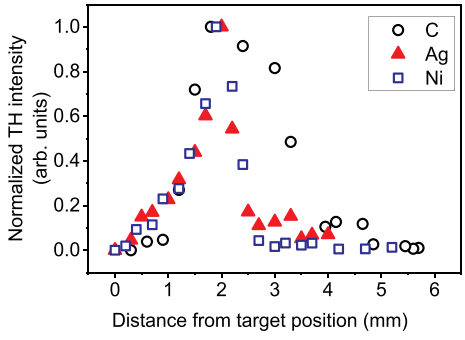

Fig. 2. Normalized TH intensity as a function of the distance between the axis of propagation of the probe pulses and C, Ag, and Ni surfaces at constant ps heating pulse energy (0.56 mJ) and fs probe pulse energy (0.045 mJ).

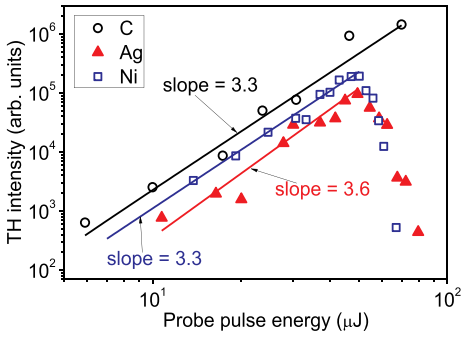

Fig. 3. TH intensity as a function of the probe pulse energy at the constant ps heating pulse energy of 0.56 mJ operating at 1 kHz on the surfaces of ablating C, Ag, and Ni targets.

number of free electrons due to the interaction of intense fs probe pulses with the ejected particles during ablation, which led to the phase mismatch between the probe (800 nm) and TH (266 nm) waves in the plasma area. However, up to the pulse energy of 70 μJ, TH intensity showed the cubic dependence in case of C plasma. This difference in the variation of TH yields of three plasmas shows that the employed probe energy of 70 μJ for the generation of TH is far from the threshold limit for free-electron generation in the case of C plasma. The absence of a decrease in TH intensity upon the increase of probe pulse energy beyond 50 μJ for C as compared to Ag and Ni can be related with the ionization energies of used atoms, which is higher for C (11.26 eV) and relatively smaller for Ag (7.57 eV) and Ni (7.6 eV). Notice that the second ionization potentials of C, Ag, and Ni are 24.38 eV, 21.48 eV, and 18.48 eV, which also points out the smaller probability for further ionization for C than Ag and Ni.

The employed intensity of 0.56 mJ for 200 ps heating pulses was $\sim 1.5 \times 10^7$ Wcm^{-2}. At this intensity of heating pulses, the degree of ionization was less than 1 which indicates the appearance of neutral species/ions in the created Ag and Ni plasmas [33]. At the same time, the 50 μJ probe pulse energy corresponds to the peak intensity of $\sim 2.7 \times 10^{14}$ Wcm^{-2}. The appearance of free electrons at this intensity is due to the possibility of further ionization of singly ionized species rather in addition to the ionization of neutral species in plasma plume [34,35]. The intensity provided by the probe pulses is close to the tunnel ionization threshold for the singly charged Ag and Ni ions. However, the tunnel ionization threshold for singly charged C ions is higher than the employed probe pulse intensity. Correspondingly, C plasma should demonstrate the lesser influence of free electrons on TH yield compared with Ag and Ni plasmas at similar conditions of experiments. As a consequence of employed pulse energy and low ionization potential for the case of Ag and Ni, the increase in free-electron density led to a decrease in the intensity of TH due to the phase mismatch of the probe and TH waves.

3.2. THG from metal plasma in the vacuum

In this section, THG study in various bulk targets, such as C, Cr, Ag, In, CdS, and ZnS, ablated under a vacuum pressure of 0.1 Pa is reported. The schematic of the experiments is shown in Fig. 1(b), where ns heating pulses at 1064 nm were used for LA to create the plasma plumes. The application of ns pulses for LA provided precise control over the time delay between the heating and the probe pulses using the delay generator. Prior to these studies, TH yield from four plasmas (Ag, C, Cr, and In) at variable probe pulse energies was measured using the fixed heating pulse energy of 3 mJ (Fig. 4). The measurements of TH intensity were performed by setting the target position 0.6 mm away from the axis of the probe pulses propagation. The variations of TH intensity in studied plasmas showed approximately cubic dependences with the variation of the probe pulses energy up to the maximum used pulse

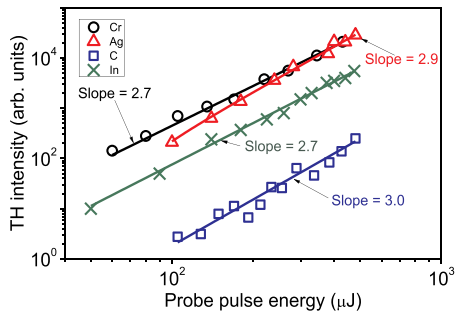

Fig. 4. TH intensity as a function of the energy of the probe pulses propagating through Ag, Cr, C, and In plasmas formed under vacuum conditions at the constant energy of ns heating pulse (3 mJ) at 10 Hz.

energies of 0.5 mJ. This observation conclude that the threshold limit for the generation of free electrons in those plasmas under vacuum conditions was far from maximal applied pulse energies, which has earlier been considered to be the dominating factor at reasonably high energies of the probe pulses [36]. Under the ns plasma in vacuum condition, TH intensity was observed to be lowest for C plasma and maximal for Ag plasma. As mentioned in the previous section, the ionization threshold of C is much higher compared to Ag, which can directly influence the plasma density. The plasma density becomes less for C as compared to Ag. Apart from contribution of ionization potential of the material under study, the decrease in plasma density can also be accredited to the employed laser pulse duration during LA. It was reported that, under the same experimental condition, the shorter pulses result in the lesser ablated mass and/or excited species in the created plasma as compared to ns pulses [37].

Fig. 5 shows the variations of TH intensity as the functions of the distance between the target and the probe pulses during ablation of Ag, Cr, In, and C targets at vacuum conditions. The generation of TH during ablation of C was observed up to ~4 mm away from the position of a target, whereas the TH intensity was achieved up to the distance of 1 mm for other three bulk targets. This study reveals the characteristics of the ejected particles, which were created during LA of different bulk targets and participated in THG. It was assumed that TH intensity depends on the distance (x) between the probe pulses propagation and target in accordance with the relation $I_{TH} \propto x^{-n}$, where n was considered to be dependent on the heating pulse intensity. From Fig. 5, TH intensity in the case of C and In was proportional to the distance from the target with the power low of $n = -1.85$ and -2.85 respectively. However, a completely different scenario was observed for the case of Cr and Ag plasmas, which showed two regions with different slopes (-1.15 and -5.9 in the case of Ag plasma, and -1.79 and -6.9 in the case of Cr plasma).

TH intensity shows a similar trend with the variation of target position up to ~0.6 mm for all targets. As the distance from targets further increases, TH intensity decreases with two different regimes of x variations. This difference can be attributed to TH intensity changes due to both the density and the length of the nonlinear medium variations, which demonstrate the inverse relationship with each other as the ejected particles propagate away from the surface of the target. To understand the TH intensity variations with the growth of distance from the target, the statistical distribution of each group of particles during plasma formation should be analyzed, similar to earlier reported studies [25]. The dependence of TH intensity on the probe distance from the surface of the target has shown the presence of different species with different masses and velocities during the formation of plasma that has a direct impact on TH yield. This is largely governed by the motion of the ejected particles away from the surface of the ablated target while considering the energy conservation during LA. This leads to the conclusion that during LA of the bulk target, lighter particles, such as C and Ag, are responsible for the generation of TH at larger distances from the target.

Similar to TH intensity variation in Ag and Cr plasmas, the TH intensity in CdS and ZnS plasmas shows a similar trend with the variation of the distance between the target and the probe pulses (Fig. 6). To explain TH intensity variations in all plasmas shown in Figs. 5 and 6, the presence of two groups of particle clouds is assumed, which have been observed previously in different materials [28]. Their presence can be explained by the fact that the ablation of the outermost surface of targets results in atomization, whereas the inner surface is responsible for the generation of molecules, clusters, and nanoparticles due to the explosion and mechanical fragmentation processes. These atomic and clustered clouds of particles move towards the probe beam with different velocities, which was observed during THG studies. This peculiarity can be the dominating factor for the TH intensity behavior in the case of Ag, Cr, CdS and ZnS. From this trend of TH intensity variations, one can observe the ejected cloud of particles containing few atom-sized clusters or large nanoparticles during the creation of plasma. These clusters and nanoparticles travel smaller distance compared to the generated atoms and ions during the creation of plasma.

TH intensity was analyzed as a function of a time delay between the heating and the probe pulses under vacuum conditions. To measure the dependence of TH intensity on the variation of the delay between the heating and the probe pulses, the target sample was placed at the focus of the heating pulses and 0.6 mm away from probe pulses. The pulse energies of the heating and the probe pulses were maintained at 3 and 0.50 mJ respectively. The comparison of TH intensity at variable delay was carried out for C, Cr, Ag, and In plasmas. Fig. 7(a) shows the modulation of TH yield with the variation of the delay between the heating and the probe pulses. TH intensity shows the similar trend with delay variations for all samples with TH maxima observed at 90 ns (C), 180 ns (Cr), 200 ns (Ag) and 250 ns (In). The TH intensity decreases slowly after reaching a maximum as the delay time increases. The

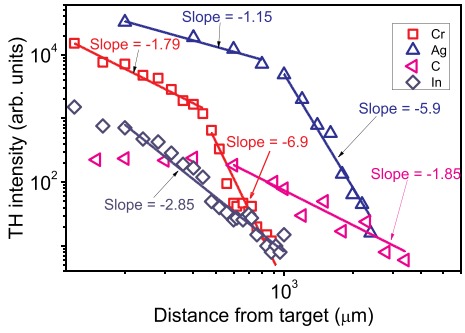

Fig. 5. TH intensity as a function of the distance between the surface of the bulk target (Ag, Cr, In, and C) and the probe pulses at the constant heating pulse energy (3 mJ) and probe pulse energy (0.5 mJ).

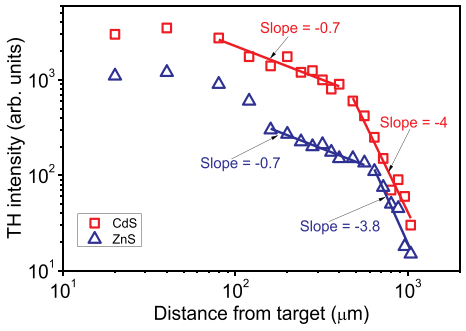

Fig. 6. TH intensity as a function of the distance between the surfaces of bulk CdS and ZnS and the probe pulses at the constant pulse energy of 3 mJ for ns heating pulses and 0.5 mJ for fs probe pulses.

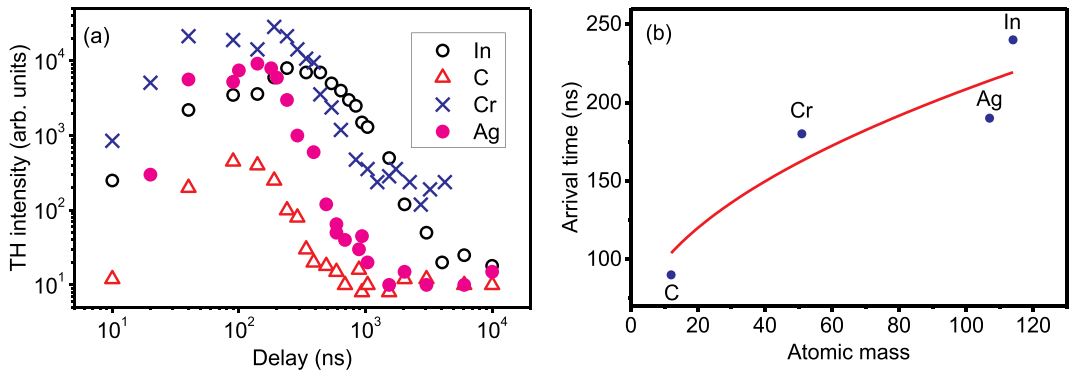

Fig. 7. (a) TH intensity as a function of the delay between the heating and the probe pulses. (b) the arrival time of C, Cr, Ag, and In particle clouds at the area of propagation of the probe pulses when TH intensity maxima were observed. The solid curve represents the phenomenological fit of the relationship between the delay time and atomic mass ($t_d \propto M^{0.5}$).

variations of TH intensity with delays time are in good agreement with the earlier reported studies [28]. These measurements show that the atomic and the ionic species are the dominant components responsible for HG at present conditions compared with the clusters and nanoparticles in plasmas. The optical emission spectra of these species (see Fig. 9(a)) clearly indicate the atomization of bulk materials during heating by ns pulses. It is worth mentioning the objective of this study is to look into the impact of the type of bulk materials on TH intensity variations. We correlated the delay times at which maximal yields of TH were achieved with their respective masses [Fig. 7(b)]. The atomic mass of the ablated target has a direct effect on the arrival time of the ejected particle at the probe pulse axis. Thus, HG in plasmas provides an assessment of the particle size distribution for different materials.

The HG in plasma can provide information about the role of the complex composition of ablated species. The nature of HG emitters can be revealed by the evolution of the harmonic yield towards the maximum at some specific delay from the beginning of laser ablation. This specific delay, at fixed heating pulse energy, can be used to characterize the propagation time needed for the cluster/molecules to reach the probe pulse axis. The components created during LA can be characterized using their average arrival times [25], which can be assigned to different cluster sizes governed by conservation of average kinetic energy ($E = mv^2/2$). A relationship between employed energies and the mass of ejected particles govern the relationship between the arrival time and the masses of ejected particles. The delay at which TH yield reaches its maximum should scale as a square root of atomic weight, e.g. $t_d \propto M^{0.5}$. It reflects the lighter atoms and ions from the target surface will reach the probe pulse position before the heavier species.

Following this logic, due to the kinetic relation of particles movement, the large clusters/aggregates should appear in the laser-plasma interaction zone $n^{0.5}$ times later than single atoms and ions of respective materials, where b = m/M, b correspond to the number of atoms in the clusters/aggregates having weight m. In other words, the appearance of the group of clusters in the interaction zone could be expected at delayed times compared to the lighter particles. To validate the relationship between the arrival time and the atomic masses of materials, the temporal evolution of the TH yield from various plasmas was analyzed, as shown in Fig. 7(a). As mentioned above, the distance between target and fs beam propagation in these experiments was maintained at ~0.6 mm. As expected, the arrival times for atomic and ionic species of Cr, In and Ag were $(M_{Cr}:M_C)^{0.5}$~1.27, $(M_{In}:M_C)^{0.5}$~3 and $(M_{Ag}:M_C)^{0.5}$~2.9 times longer compared with the optimal delay for C particles. This anticipated maximal yield of TH from respective plasmas was observed in our experiments as shown in Fig. 7(b).

The evolution of TH intensity with the variation of delay between the heating and the probe pulses has been studied theoretically and experimentally in Refs. [25,28]. It is indicated that the TH intensity variations at $t_d < 300$ ns are possibly due to the presence of ions and neutral atoms. The TH intensity variations at the delays greater than 300 ns can be attributed to the presence of clusters and nanoparticles in the plasma. Under experimental conditions, the optical emission from plasma consists of the emission line attributed to the respective ions [see Fig. 9(a)]. It is supported by the fact that the initial variation of TH intensity with delay is typically due to the presence of atoms and ions during plasma formation.

To demonstrate the relationship between the arrival times of the ejected particles and their masses, TH intensity as a function of time delay was measured during LA of the wide-bandgap semiconductors (CdS and ZnS). Fig. 8 shows that TH intensities reach the maximums at the delays of 540 ns (ZnS) and 690 ns (CdS). This observation also supports the relationship between arrival times and atomic masses. The expected arrival time for CdS atoms, ions or clusters is $(M_{ZnS}:M_{CdS})^{0.5}$~1.22 times longer than the arrival time of ZnS species. TH in these plasmas was observed up to the delays of 2 μs that was in agreement with literature at the target distance of 0.6 mm from the probe pulse position [27,28,38].

The optical emission spectra from the CdS and ZnS plasmas revealed the existence of atomic species like Cd, Zn, S, and their respective ions in the plasma area [Fig. 9(b)]. The complex mixture of Cd(II) and Cd(I) was observed in optical emission spectra of CdS plasma. However, the emission spectra from ZnS plasma show the emission lines attributed to Zn(I). These emission lines showing the presence of neutal and ionic species present in plasma from CdS and ZnS are mosly responsible for the TH yield at earlier time scale as compared to agreegates and clusters.

The TH intensity approaches its maximum at around 100–300 ns for C, Ag, Cr and In, which is an earlier timescale compared to the timescales of 540 ns for CdS and 690 ns for ZnS. These time scales can be better explained by the fact that the created plasmas contain two components. One consists of atoms and ions, which can possess the velocity at around 5×10^5 cm s^{-1}, and the other consists of clusters and

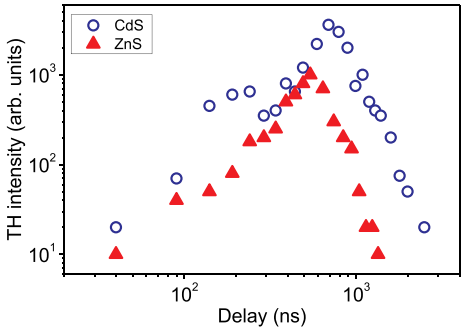

Fig. 8. TH intensities as the functions of the delays between ns heating and the probe pulses in the case of CdS and ZnS plasmas.

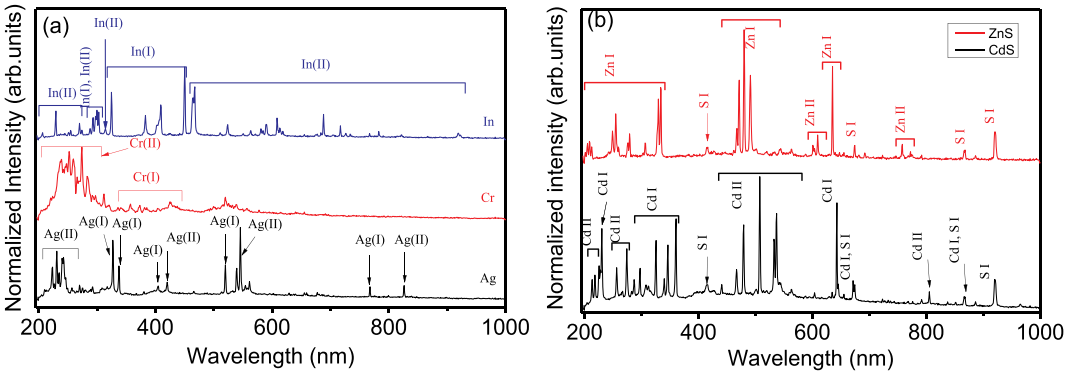

Fig. 9. Emission spectra of the studied plasmas excited by ns heating pulses (3 mJ). (a) Ag, Cr, and In. (b) CdS and ZnS.

nanoparticles with the respective velocities of $1 \times 10^5\,\mathrm{cm\,s^{-1}}$. TH intensity variations in semiconductor materials are presumably due to the existence of large-sized clusters and nanoparticles as compared to atoms or ionic species in the metal plasma. This is because the larger sized cluster and particle arrive at a longer time scale as compared to atomic and ionic species.

4. Conclusions

THG in various plasma targets was studied using nanosecond and picosecond heating pulses in both vacuum and air. TH from various plasmas was used as a probe to characterize the components of the plasma. TH intensity shows the cubic dependence on the probe pulse energy in both air and vacuum. It was observed that, in air, TH intensity decreases with the increase of the probe pulses energy at higher intensity regime, which is an indication of free electron generation in plasma under the influence of air due to high probe pulse fluence. TH intensity variations with the distance between the target and the probe pulses reveal the nature of the ejected particles during ablation under vacuum conditions, which was not observed during THG in air. TH intensity measurements with the change of the distance between the target surface and the probe pulses position have shown the significant contribution of the smaller sized particles along with ions and atoms compared to the heavier particles. The modulation of TH intensity with the variation of delay between the heating and probe pulses is attributed to the influence of the masses of ejected particles in accordance with the relation $t_d \propto M^{0.5}$. Among the studied materials under vacuum conditions, the relative TH conversion efficiency is larger for Ag plasma compared to the other species. We have shown that THG in metal plasmas is governed by the atomic or ionic species, contrary to the wide-bandgap semiconductor materials where TH was generated by the small-sized clusters and nanoparticles. TH maxima were observed at the delays in the range of 100–300 ns for metal plasmas as compared 500–700 ns for semiconducting materials. This difference in optimal delays has revealed that, during LA, the ejected particles from metal targets move faster compared to heavier targets. This study can be generalized to a variety of different materials as the sources of plasma for THG depending on the delay and spatial spreading of the plasma expansion.

Data availability

The data used in this article to support the findings of this study are available from the corresponding author upon request.

Declaration of competing interest

The authors declare that they have no known competing financial interests or personal relationships that could have appeared to influence the work reported in this paper.

Acknowledgments

The financial support from the Natural Science Foundation of China (61774155, 61705227) and National Key Research and Development Program of China (2017YFB1104700) is appreciated. R.A.G. thanks the financial support from the Chinese Academy of Sciences President's International Fellowship Initiative (Grant No. 2018VSA0001).

Appendix A. Supplementary data

Supplementary data to this article can be found online at https://doi.org/10.1016/j.optmat.2019.109423.

References

[1] H.S. Choi, J.V. Frangioni, Nanoparticles for biomedical imaging: fundamentals of clinical translation, Mol. Imaging 9 (2010) 291–310.
[2] J. Li, T. Zhao, T. Chen, Y. Liu, C.N. Ong, J. Xie, Engineering noble metal nanomaterials for environmental applications, Nanoscale 7 (2015) 7502–7519.
[3] Z.L. Wang, W. Wu, Nanotechnology-enabled energy harvesting for self-powered micro-/nanosystems, Angew. Chem. 51 (2012) 11700–11721.
[4] S.L. Pal, U. Pal, P.K. Manna, G.P. Mohanta, R. Manavalan, Nanoparticle: an overview of preparation and characterization, J. Pharm. Sci. 1 (2011) 228–234.
[5] A.B. Sharma, M. Sharma, R.K. Pandey, Synthesis, properties and potential applications of semiconductor quantum particles, Asian J. Chem. 21 (2009) S033–S038.
[6] W. Chang, G. Skandan, H. Hahn, S.C. Danforth, B.H. Kear, Chemical vapor condensation of nanostructured ceramic powders, Nanostructured Mater. 4 (1994) 345–351.
[7] M.D. Shirk, P.A. Molian, A review of ultrashort pulsed laser ablation of materials, J. Laser Appl. 10 (1998) 18–28.
[8] M. Kim, S. Osone, T. Kim, H. Higashi, T. Seto, Synthesis of nanoparticles by laser ablation: a review, Phys. Rev. Lett. 69 (1992) 2176.
[9] C.-Y. Shih, R. Streubel, J. Heberle, A. Letzel, M.V. Shugaev, C. Wu, M. Schmidt, B. Gokce, S. Barcikowski, L.V. Zhigilei, Two mechanisms of nanoparticle generation in picosecond laser ablation in liquids: the origin of the bimodal size distribution, Nanoscale 10 (2018) 6900–6910.
[10] P. Ecija, M.N. Sánchez Rayo, R. Martínez, B. Sierra, C. Redondo, F.J. Basterretxea, F. Castaño, Fundamental processes in nanosecond pulsed laser ablation of metals in vacuum, Phys. Rev. A 77 (2008), 032904.
[11] S. Amoruso, R. Bruzzese, X. Wang, N.N. Nedialkov, P.A. Atanasov, Femtosecond laser ablation of nickel in vacuum, J. Phys. D Appl. Phys. 40 (2007) 331.
[12] S. Noel, J. Hermann, T. Itina, Investigation of nanoparticle generation during femtosecond laser ablation of metals, Appl. Surf. Sci. 253 (2007) 6310–6315.
[13] S. Mourdikoudis, R.M. Pallares, N.T.K. Thanh, Characterization techniques for nanoparticles: comparison and complementarity upon studying nanoparticle properties, Nanoscale 10 (2018) 12871–12934.
[14] B. Kearton, Y. Mattley, Laser-induced breakdown spectroscopy: sparking new applications, Nat. Photonics 2 (2008) 537–540.
[15] Q. Cui, R.A. Muniz, J.E. Sipe, H. Zhao, Strong and anisotropic third-harmonic generation in monolayer and multilayer ReS_2, Phys. Rev. B 95 (2017) 165406.
[16] U. Petzold, A. Büchel, T. Halfmann, Effects of laser polarization and interface orientation in harmonic generation microscopy, Opt. Express 20 (2012) 3654–3662.
[17] M. Lopez-Arias, M. Oujja, M. Sanz, R.A. Ganeev, G.S. Boltaev, N. Kh Satlikov, R. I. Tugushev, T. Usmanov, M. Castillejo, Low-order harmonic generation in metal ablation plasmas in nanosecond and picosecond laser regimes, J. Appl. Phys. 111 (2012), 043111.
[18] T. Ozaki, L.B. ElougaBom, R. Ganeev, J.-C. Kieffer, M. Suzuki, H. Kuroda, Intense harmonic generation from silver ablation, Laser Part. Beams 25 (2007) 321–327.

[19] I. Hartinger, R.A. Bartels, Enhancement of third-harmonic generation by a laser-induced plasma, Appl. Phys. Lett. 93 (2008) 151102.
[20] R.A. Ganeev, G.S. Boltaev, T. Usmanov, Third and fourth harmonics generation in laser-induced periodic plasmas, Opt. Commun. 314 (2014) 114–119.
[21] R.A. Ganeev, V.I. Redkorechev, T. Usmanov, Optical harmonics generation in low-temperature laser produced plasma, Opt. Commun. 135 (1997) 251–256.
[22] I. Lopez-Quintas, M. Oujja, M. Sanz, M. Martín, R.A. Ganeev, M. Castillejo, Low-order harmonic generation in nanosecond laser ablation plasmas of carbon containing materials, Appl. Surf. Sci. 278 (2013) 33–37.
[23] R.P. Singh, S.L. Gupta, R.K. Thareja, Third harmonic generation in air ambient and laser ablated carbon plasma, Phys. Plasmas 22 (2015) 123302.
[24] R.A. Ganeev, High-Order Harmonic Generation in Laser Plasma Plumes, Imperial College Press, 2012.
[25] M. Oujja, J.G. Izquierdo, L. Banares, R. de Nalda, M. Castillejo, Observation of middle-sized metal clusters in femtosecond laser ablation plasmas through nonlinear optics, Phys. Chem. Chem. Phys. 20 (2018) 16956–16965.
[26] R. de Nalda, M. Lopez-Arias, M. Sanz, M. Oujjaa, M. Castillejo, Harmonic generation in ablation plasmas of wide bandgap semiconductors, Phys. Chem. Chem. Phys. 13 (2011) 10755–10761.
[27] M. Sanz, M. Lopez-Arias, J.F. Marco, R. de Nalda, S. Amoruso, G. Ausanio, S. Lettieri, R. Bruzzese, X. Wang, M. Castillejo, Ultrafast laser ablation and deposition of wide bandgap semiconductors, J. Phys. Chem. C 115 (2011) 3203–3211.
[28] M. Sanz, R. de Nalda, J.F. Marco, J.G. Izquierdo, L. Banares, M. Castillejo, Femtosecond pulsed laser deposition of nanostructured CdS films, J. Phys. Chem. C114 (2010) 4864–4868.
[29] R.A. Ganeev, G.S. Boltaev, R.I. Tugushev, T. Usmanov, M. Baba, H. Kuroda, Third harmonic generation in plasma plumes using picosecond and femtosecond laser pulses, J. Opt. 12 (2010), 055202.
[30] W.R. Creasy, J.T. Brenna, Large carbon cluster ion formation by laser ablation of polyimide and graphite, Chem. Phys. 126 (1988) 453–468.
[31] M. Kim, S. Osone, T. Kim, H. Higashi, T. Seto, Synthesis of nanoparticles by laser ablation: a review, KONA Powder and Particle J 34 (2017) 80–90.
[32] N.G. Semaltianos, Nanoparticles by laser ablation, Crit. Rev. Solid State Mater. Sci. 35 (2010) 105–124.
[33] L.B. ElougaBom, J.-C. Kieffer, R.A. Ganeev, M. Suzuki, H. Kuroda, T. Ozaki, Influence of the main pulse and prepulse intensity on high-order harmonic generation in silver plasma ablation, Phys. Rev. A 75 (2007), 033804.
[34] T. Ozaki, L.B. ElougaBom, R. Ganeev, J.-C. Kieffer, M. Suzuki, H. Kuroda, Intense harmonic generation from silver ablation, Laser Part, Beams 25 (2007) 321–327, 2007.
[35] R.A. Ganeev, H. Singhal, P.A. Naik, U. Chakravarty, V. Arora, J.A. Chakera, R. A. Khan, M. Raghuramaiah, S.R. Kumbhare, R.P. Kushwaha, P.D. Gupta, Optimization of the high-order harmonics generated from silver plasma, Appl. Phys. B 87 (2007) 243–247.
[36] G. Lambert, A. Andreev, J. Gautier, L. Giannessi, V. Malka, A. Petralia, S. Sebban, S. Stremoukhov, F. Tissandier, B. Vodungbo, P. Zeitoun, Spatial properties of odd and even low order harmonics generated in gas, Sci. Rep. 5 (2015) 7786.
[37] J. Thomas, H.C. Joshi, A. Kumar, R. Philip, Pulse width dependent dynamics of laser induced plasma from a Ni thin film, J. Phys. D Appl. Phys. 52 (2019) 135201.
[38] M. Oujja, I. Lopez Quintas, A. Benitez Canete, R. de Nalda, M. Castillejo, A. B. Canete, Harmonic generation by atomic and nanoparticle precursors in a ZnS laser ablation plasma, Appl. Surf. Sci. 392 (2017) 572–580.